158–171 *Nucleic Acids Research, 2009, Vol. 37, No. 1* *Published online 25 November 2008*
doi:10.1093/nar/gkn914

Loop 2 in *Saccharomyces cerevisiae* Rad51 protein regulates filament formation and ATPase activity

Xiao-Ping Zhang[1], Vitold E. Galkin[2], Xiong Yu[2], Edward H. Egelman[2] and Wolf-Dietrich Heyer[1,3,*]

[1]Department of Microbiology, University of California, Davis, CA 95616-8665, [2]Department of Biochemistry and Molecular Genetics, University of Virginia, Box 800733, Charlottesville, VA 22908 and [3]Department of Molecular and Cellular Biology, University of California, Davis, CA 95616-8665, USA

Received September 22, 2008; Revised October 16, 2008; Accepted October 29, 2008

ABSTRACT

Previous studies showed that the K342E substitution in the *Saccharomyces cerevisiae* Rad51 protein increases the interaction with Rad54 protein in the two-hybrid system, leads to increased sensitivity to the alkylating agent MMS and hyper-recombination in an oligonucleotide-mediated gene targeting assay. K342 localizes in loop 2, a region of Rad51 whose function is not well understood. Here, we show that Rad51-K342E displays DNA-independent and DNA-dependent ATPase activities, owing to its ability to form filaments in the absence of a DNA lattice. These filaments exhibit a compressed pitch of 81 Å, whereas filaments of wild-type Rad51 and Rad51-K342E on DNA form extended filaments with a 97 Å pitch. Rad51-K342E shows near normal binding to ssDNA, but displays a defect in dsDNA binding, resulting in less stable protein-dsDNA complexes. The mutant protein is capable of catalyzing the DNA strand exchange reaction and is insensitive to inhibition by the early addition of dsDNA. Wild-type Rad51 protein is inhibited under such conditions, because of its ability to bind dsDNA. No significant changes in the interaction between Rad51-K342E and Rad54 could be identified. These findings suggest that loop 2 contributes to the primary DNA-binding site in Rad51, controlling filament formation and ATPase activity.

INTRODUCTION

Homologous recombination (HR) is an important pathway in maintaining genomic stability. HR leads to repair or tolerance of complex DNA lesion, including gaps, double stranded breaks (DSBs), interstrand crosslinks, involving a template-switching mechanism that allows a broken or stalled 3′-end to continue template-directed DNA synthesis (1–3). The RecA family of proteins catalyzes the key reactions of HR: homology search and DNA strand invasion (4).

RecA protein (and its viral, archaeal and eukaryotic counterparts) form ternary complexes with ATP and ssDNA termed the presynaptic filament, which serves as a catalytic surface for the homology search process (5). The exact process, by which RecA identifies homology in the duplex target DNA remains to be determined, but likely involves flipping of bases in the target duplex DNA to allow alternative pairing with the RecA-bound ssDNA (6,7). RecA protein has two DNA-binding sites (8). The primary site is utilized for filament formation, and saturates at a stoichiometry of 3 nt per RecA protomer. The secondary binding site accommodates the target dsDNA for the homology search and stabilizes the heteroduplex DNA, the product of DNA strand exchange (9,10). The original RecA crystal structure provided a framework to define the structural underpinning of the DNA-binding sites (11). Two disordered loops, L1 (RecA residues 157–164) and L2 (residues 195–209), that remained undefined in the original structure were proposed to be involved in DNA binding (11). These loops were predicted to project towards the central axis of the filament (11), where DNA has been proposed to reside on the basis of electron microscopic (EM) studies (12,13). Also mutant and crosslinking studies failed to provide a consistent assignment of the primary or secondary DNA-binding sites to L1 or L2 [see Discussion section, for review (4)]. The recently determined structures of RecA filaments on ssDNA and dsDNA authoritatively bear out these predictions (14). Both structures show that L1 and L2 become ordered and bind DNA in the confines of the filaments. The structures of the phosphodiester backbones in the

*To whom correspondence should be addressed. Tel: +1 530 752 3001; Fax: +1 530 752 3011; Email: wdheyer@ucdavis.edu

presynaptic (ssDNA) and postsynaptic (dsDNA) filaments are very similar, showing triplets of 3 nt/base pairs with significant underwinding between the triplets. This leads to non-isotropic extension of the DNA by 50% to ~18.5 nucleotides or base pairs per turn and and an average rise of ~5.1 Å per nucleotide or base pair, consistent with the previous EM studies (12,13). The complementary strand of the duplex DNA is primarily held in place by Watson–Crick interactions with few specific protein contacts, making heteroduplex formation strictly dependent on base pairing complementarity. The structures of the RecA-ssDNA and dsDNA filaments provide a basis to start understanding the mechanism of RecA-mediated homology search and serve as a paradigm for the eukaryotic Rad51 protein.

Rad51 is the eukaryotic homolog of the bacterial RecA protein (4). The overall structure of the protein and the filament on DNA is well conserved, although the C-terminal DNA-binding region of RecA protein appears to have been transposed to the N-terminus in the Rad51 proteins (15–18). The budding yeast Rad51 protein contains an exceptionally long N-terminus, which was truncated to the size more typical of eukaryotes to derive crystals for the structural analysis (15). In the Rad51 structure L1 (*Saccharomyces cerevisiae* Rad51 residues 288–294**)** and L2 (residues 327–344) could not be defined, presumably due to disorder (15). Rad51 mutant studies fail to provide a clear picture on the participation of L1 and L2 in ssDNA and dsDNA binding in the primary or secondary binding site (see Discussion section). Despite their overall similarity, RecA and Rad51 also exhibit significant differences in their biochemical properties and it is likely that these differences have a structural basis. Unlike RecA protein, Rad51 protein does not show a kinetic delay binding to dsDNA, displaying only a modest preference for ssDNA (19). Moreover, Rad51 displays a significantly (100–200-fold) reduced ATPase activity when bound to ssDNA or dsDNA in comparison with RecA. Both proteins gain their high-affinity binding state, when bound to ATP. While RecA attains the lowest affinity after ATP hydrolysis in the ADP-bound state, Rad51 exhibits its lowest DNA-binding affinity in the absence of nucleotide (4). These differences have significant consequences for the dynamic behavior of the proteins binding and releasing DNA in conjunction with the nucleotide cofactor cycle, but the structural underpinnings of these differences are unknown.

The Rad51-K342E mutation provides an excellent opportunity to study the function of L2 in Rad51 protein. This mutant was found to enhance the interaction of Rad51 protein with Rad54 protein in the two-hybrid system, without affecting Rad51's interaction with Rad52, Rad55, or itself (20). This mutant did not fully complement the MMS-sensitivity of a *rad51* deletion strain, suggesting a partial loss of function (20). Intriguingly, this mutant enhanced recombination between an oligonucleotide and a plasmid-borne gene, when overexpressed in wild-type cells, suggesting a hyper-rec phenotype (21). An alanine substitution at the analogous of the hRad51 protein (K284A) was found to have little effect on dsDNA binding (22). Here, we show that the Rad51-K342E mutation has a significant impact on dsDNA binding. Importantly, the mutant protein forms filaments in the absence of a DNA lattice that are competent for ATP hydrolysis. These data suggest that L2 of Rad51 is part of the primary DNA-binding site and that L2 is key to coordinate ATP binding with DNA binding and filament formation.

MATERIALS AND METHODS

Yeast media, strains and plasmids

Standard yeast media were used for cell growth. *S. cerevisiae* WDHY1930 (*MATa his3-Δ1 leu2-3,112 trp1 ura3-52 pep4-3 rad51-Δ::KanMX*) was the expression host for the expression of mutant Rad51 proteins. Rad51-K342E and Rad51-K191R,K342E expressing plasmids were obtained by PCR-mediated site-directed mutagenesis (23) using pR51.3 plasmid [a kind gift from Patrick Sung, Yale University (24)] as template. The forward mutagenesis primer for Rad51-K342E was 5′-GGT GGTATGGCTTTTAATCCAGATCCAGAAAAGCCT ATCGGTGG-3′ and the reverse primer 5′-CCACCGAT AGGCTTTTCTGGATCTGGATTAAAAGCCATACC ACC-3′. The respective primers for the K191R mutation were 5′-TTCAGGACAGGTCGGTCCCAGCTATG TCACACTTTGGCCG-3′ and 5′-CGGCCAAAGTGT GACATAGCTGGGACCGACCTGTCCTGAA-3′. The sequences of the entire genes were confirmed by DNA sequencing.

Protein overexpression and purification

GST-Rad54 and RPA were purified as described previously (25). The wild-type Rad51, Rad51-K191R, Rad51-K342E and Rad51-K342E,K191R proteins were purified as described (26).

DNA substrates

RFI ϕX174 and ϕX174 virion DNAs were purchased from New England Biolabs Inc. Polynucleotides [poly(dT), poly(dA), poly(dC)] were purchased from Amersham Pharmacia Biotech. Linearized ϕX174 dsDNA was produced by cleavage of RFI ϕX174 by *Pst*I.

ATPase activity

A charcoal-based ATPase assay was used as described (23,25). Briefly, the reaction buffer contained 33 mM Tris–HCl, pH 7.5, 13 mM $MgCl_2$, 1.8 mM DTT, 1 mM ATP, 90 μg/ml BSA. DNA and protein concentrations were varied as indicated. A 50 μl reaction system contained 0.1 μCi [γ-^{32}P]-ATP. The free [γ-^{32}P] from [γ-^{32}P]-ATP hydrolysis was counted on a Beckman LS6500 multipurpose scintillation counter. The ATPase activity is expressed as the ratio of radioactivity in free phosphate relative to the total radioactivity added in the sample after 30 min incubation. The ATPase activity of wild-type Rad51 and Rad51-K342E protein is linear up to 60 min in the presence and absence (Rad51-K342E only) of DNA (data not shown). Hence, the data are reflective of the ATPase rate.

DNA strand exchange assay

The DNA strand exchange reaction was performed as described (25). The reaction buffer contained 30 mM Tris–acetate, pH 7.5, 1 mM DTT, 20 mM ATP, 20 mM magnesium acetate, 2 mM phosphocreatine, 0.1 μg/μl creatine kinase, 50 μg/ml BSA, 2.37 mM spermidine. The reaction was started with a buffer containing 33 μM (nt) ϕX174 ssDNA and the indicated amount of Rad51 proteins in total volume of 10.5 μl. After incubation at 30°C for 15 min, 1.8 μM RPA was added and incubation was continued at 30°C for another 30 min. At this point, linearized ϕX174 dsDNA (33 μM bp) was added and incubation was continued at 30°C for 4 h. The reaction was stopped by adding 2 μl stop buffer (0.714% SDS, 357 mM EDTA and 4.3 mg/ml proteinase K) and incubated at 30°C for another 20 min. Finally, the sample was separated on a 0.8% agarose gel, stained with ethidium bromide, visualized on Eagle Eye II (Stratagene). In the modified protocol (Figure 6B), the ssDNA and dsDNA were co-incubated with Rad51 for 15 min, then RPA was added and the incubation continued for 5 h.

DNA-binding assay

A nucleoprotein gel assay was used to analyze the DNA-binding activity of the Rad51 proteins. The method is based on a difference in electrophoretic mobility of glutaraldehyde-fixed DNA-Rad51 complexes, which is related to the nucleoprotein filament saturation (27). Thirty micromolars (bp/nt) of linear ϕX174 dsDNA or circular ssDNA were used with the indicated amounts of proteins as described (23), except for the presence of different nucleotide cofactors (5 mM ATP, ATP-γ−S, or ATP + AlF_4^-). In the experiment performed with ATP + AlF_4^-, dsDNA and Rad51 were incubated with ATP (5 mM) for 15 min, then $Al(NO_3)_3$ and NaF were added to a final concentration of 5 mM. The reaction mixtures were incubated at 30°C for 30 min to form protein–DNA complexes. The complexes were separated on 0.8% agarose gels and visualized either directly or after glutaraldehyde fixation (30 min at 30°C with a final concentration of 0.25%) through ethidium bromide staining, as described (23).

Electron microscopy and three-dimensional image reconstruction

Protein-dsDNA complexes were formed in 25 mM Triethanolamine–HCl (Fisher) buffer (pH 7.2) with an incubation at 30°C for 10 min, with Rad51-K342E or wild-type Rad51 (2 μM), a protein to calf thymus dsDNA (Sigma) ratio of 40:1 (w/w), ATP (1.25 mM), NaF (1.25 mM) and $Al(NO_3)_3$ (1.25 mM) were present. The protein complexes without DNA were formed under the same conditions except that the DNA was omitted and the Rad51-K342E concentration was 5 μM. All samples were applied to a carbon film and negatively stained with 2% (w/v) uranyl acetate. The samples were imaged in a Tecnai 12 electron microscope at an accelerating voltage of 80 keV and magnification on film (Kodak SO163) of 30 000×. Negatives were scanned with a Nikon Coolscan 800 as 16-bit images using a raster of 4.2 Å/pixel. Reconstructions were generated using the IHRSR algorithm (28).

Structure analysis and molecular modeling

Sequence alignment was done in Clustalx 1.83 (29) and the alignment (Figure 1B) was visualized in Bioedit (30). The X-ray crystal structure of *S. cerevisiae* Rad51-I345T (1SZP) (15) was used as a template for the molecular models of the Rad51-K342E monomer and Rad51-K342E filament in Modeller8v2 and Modeller9v2 (31,32), respectively. The quality of the models was verified by Procheck (33), Whatif (34), ProsaII (35) and Verify_3D (36,37). The structural models (Figure 1C) were visualized in PyMol (http://www.pymol.org).

RESULTS

Loop 2 projects into the central axis of the Rad51 filament

Based on its *in vivo* phenotypes, the Rad51-K342E affords a unique opportunity to elucidate the function of L2 in the Rad51 protein. Structurally, the position of L2 is completely conserved among all RecA family members (38) (Figure 1B). The L2 sequence shows a high degree of sequence conservation among eukaryotes and contains between 17 and 19 amino-acid residues (Figure 1B). There is less conservation in L2 sequence between eukaryotes and bacteria or archaea, where the loop is also shorter (15 residues in the examples in Figure 1B). Rad51-K342 is one of two lysine residues found towards the C-terminal end of loop 2, which are well conserved in eukaryotes except plants and protozoa (for example *Cryptosporidium* in Figure 1B).

Structures for Rad51-K342E and the Rad51-K342E filament (Figure 1C and D) are based on the X-ray crystal structure of the budding yeast N-terminally truncated Rad51-I345T protein (15) and a model was built for L2. The purpose was to render an impression of the localization of the K342E mutation site in the monomer and filament. Although the specific structure is essentially arbitrary because of the limitation of the modeling protocols, L2 clearly projects into the proximal part of the central axis of the filament, close to the subunit-subunit interface, based on the localization of the anchor sites of L2 (Figure 1D). The Rad51-K342E mutation introduces a net −2 charge change for each protomer, decreasing significantly the overall positive charges in the major groove formed by L2 and other residues. Hence, the modeling suggests a potential effect of the K342E mutation on DNA binding and subunit–subunit interaction of Rad51, which is documented in the following.

Rad51-K342E exhibits DNA-dependent and DNA-independent ATPase activities

To determine its biochemical properties, Rad51-K342E protein was purified to apparent homogeneity from budding yeast (Figure 1A). All RecA-like proteins share a core ATPase domain and exhibit DNA-dependent

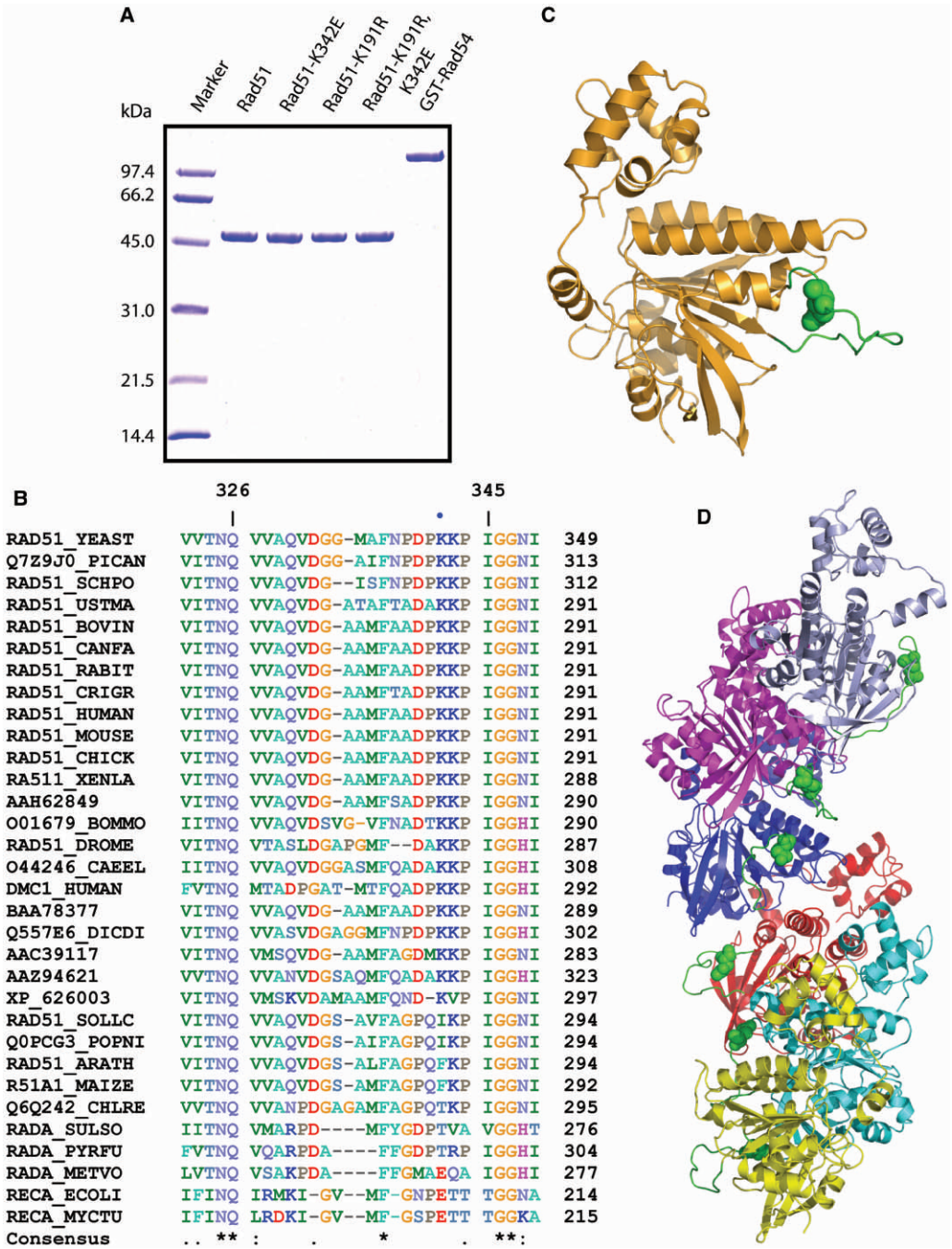

Figure 1. Purification and molecular modeling of *S. cerevisiae* Rad51-K342E protein. (**A**) Two micrograms of purified Rad51, Rad51-K342E, Rad51-K191R, Rad51-K191R,K342E and GST-tagged Rad54 proteins were visualized on 10% SDS–PAGE stained with Coomassie Blue. (**B**) Alignment of the amino acid sequences in the loop 2 regions of Rad51, RecA and RadA proteins from different organisms. The residue numbering on top is based on the *S. cerevisiae* Rad51 sequence (RAD51_YEAST). Five residues are shown on both sides of the loop 2 region and the residue number for the last residue on the right side is indicated just after the sequence. The sources are: Q7Z9J0_PICAN, yeast *Pichia angusta* (Hansenula polymorpha); RAD51_SCHPO, fission yeast, *Schizosaccharomyces pombe*; RAD51_USTMA, *Ustilago maydis* (Smut fungus); RAD51_BOVIN, *Bos taurus* (Bovine); RAD51_CANFA, *Canis familiaris* (dog); RAD51_RABIT, *Oryctolagus cuniculus* (rabbit); RAD51_CRIGR, *Cricetulus griseus* (Chinese hamster); RAD51_HUMAN, *Homo sapiens* (human); RAD51_MOUSE, *Mus musculus* (Mouse); RAD51_CHICK, *Gallus gallus* (chicken); RA511_XENLA, *Xenopus laevis* (African clawed frog); AAH62849, Zebrafish; O01679_BOMMO, *Bombyx mori* (silk moth); RAD51_DROME, *Drosophila melanogaster* (fruit fly); O44246_CAEEL, *Caenorhabditis elegans* (hypothetical protein Y43C5A.6b); DMC1_HUMAN, human DMC1; BAA78377, *Cynops pyrrhogaster* (Japanese firebelly newt); Q557E6_DICDI, Putative Rad51 from *Dictyostelium discoideum*, a soil-living amoeba; AAC39117, *Tetrahymena thermophila*, ciliate; AAZ94621, *Trypanosoma cruzi*, a parasite; XP_626003, *Cryptosporidium parvum*, an apicomplexan; RAD51_SOLLC, *Solanum lycopersicum* (tomato); Q0PCG3_POPNI, *Populus nigra* (Lombardy poplar); RAD51_ARATH, *Arabidopsis thaliana* (mouse-ear cress); R51A1_MAIZE, *Zea mays* (maize) Rad51-like protein A; Q6Q242_CHLRE, *Chlamydomonas reinhardtii*, putative Rad51; RADA_SULSO, *Sulfolobus solfataricus* RadA; RADA_PYRFU, *Pyrococcus furiosus* RadA; RADA_METVO, *Methanococcus voltae* RadA; RECA_ECOLI, *E. coli* RecA. RECA_MYCTU, RecA from *Mycobacterium tuberculosis*. The K342 residue is marked with (filled circle). 3D structural models of the *S. cerevisiae* Rad51-K342E monomer (**C**) and Rad51-K342E filament (**D**) were built based on *S. cerevisiae* Rad51-I345T X-ray crystal structure (pdb: 1SZP) (28). In the crystal structure of Rad51-I345T (1SZP), L2 was not solved probably because of its flexibility. L2 and the K342E mutation site (in sphere) are shown in green in the monomer (C) and filament (D) models to visualize the approximate localization of K342E.

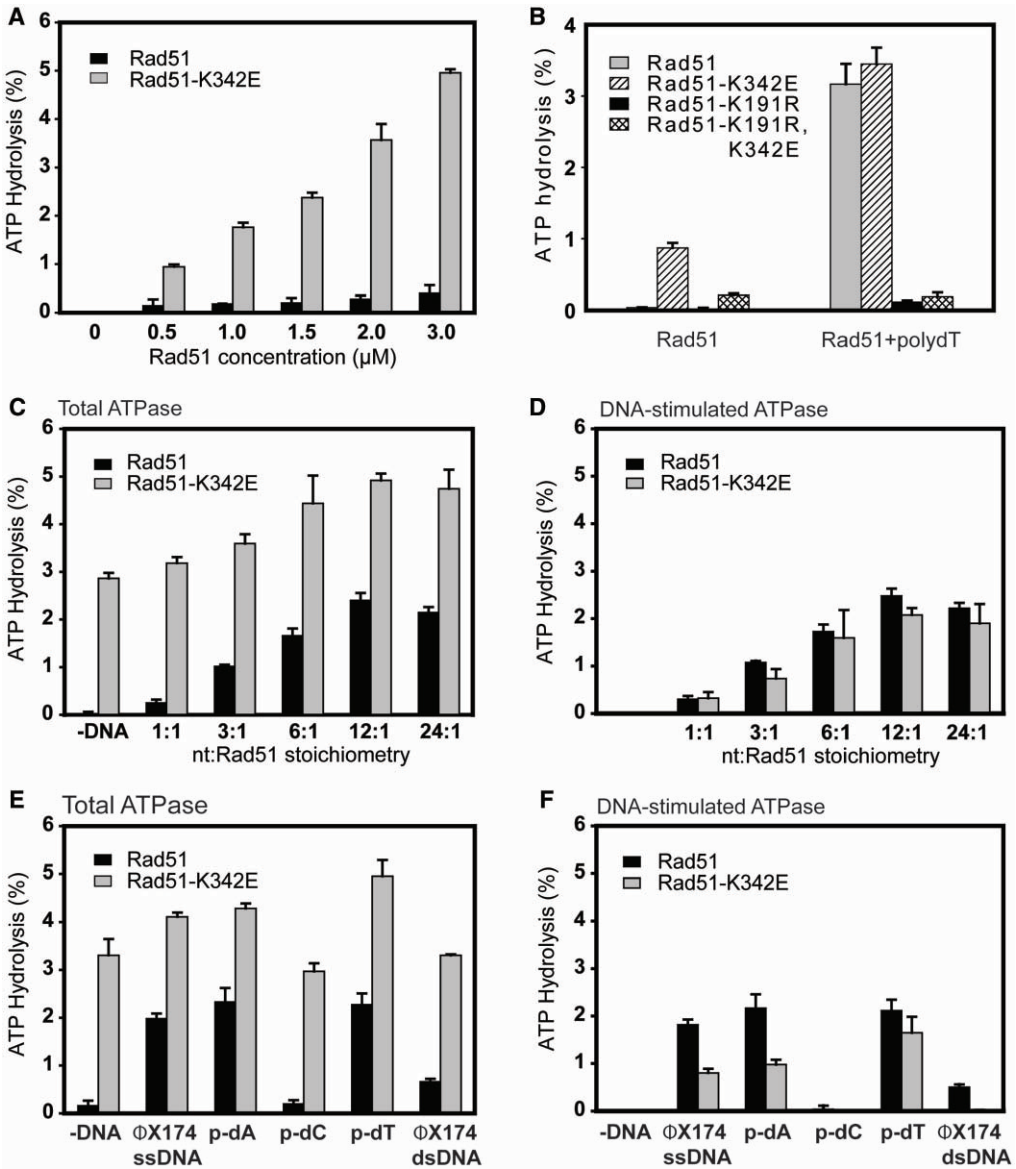

Figure 2. Rad51-K342E exhibits DNA-dependent and DNA-independent ATPase activities. (**A**) ATPase activity in the absence of DNA with varying concentrations of Rad51 or Rad51-K342E protein. (**B**) ATPase activity in the absence of DNA or in the presence of 24 μM poly(dT) at a fixed protein concentration of 2 μM for the indicated proteins. The absolute ATPase activity of Rad51-K342E protein was somewhat lower in this experiment, because it was performed not in parallel with those shown in (A, C–F). (**C**) Total ATPase activity in the presence of varying amounts of poly(dT) at a fixed protein concentration of 2 μM. (**D**) DNA-stimulated ATPase activity for conditions shown in (C), which was obtained after subtracting the ATPase activity in the absence of DNA from the values of the total ATPase activity. (**E**) Total ATPase activity of Rad51 and Rad51-K342E in response to various DNA substrates. 2 μM protein was incubated at a stoichiometry of 1:12 bp/nt with the following DNA substrates (p-dA, poly(dA); p-dC, poly(dC); p-dT, poly(dT), circular ϕX174 ssDNA and ϕX174 dsDNA). (**F**) DNA-stimulated ATPase activity for conditions shown in (E), which was obtained after subtracting the ATPase activity in the absence of DNA from the values of the total ATPase activity. Data shown are means ± 1 SD from three independent experiments.

ATPase activity. Hence, the ATPase activity has been used as an excellent surrogate for Rad51 DNA binding and filament formation (4). As demonstrated before (24), wild-type yeast Rad51 protein shows negligible ATPase activity in the absence of substrate DNA (Figure 2A). To our surprise, Rad51-K342E protein showed significant ATPase activity in the absence of DNA that increased proportionally with the amount of Rad51-K342E protein in the reaction (Figure 2A).

In several preparations, the Rad51-K342E protein purified exactly like the wild-type Rad51 protein, displaying the same chromatographic behavior (data not shown). Thus it is unlikely that a contaminant was responsible for the observed DNA-independent ATPase activity. To exclude the possibility of a contaminant, we mutated the ATP-binding site (Walker A box mutant K191R) in the Rad51-K342E protein (Figure 1A). This mutation nearly abolished the ATPase activity of the Rad51-K342E

mutant protein (Figure 2B), demonstrating that the DNA-independent ATPase activity is inherent to the Rad51-K342E protein.

The ATPase activity of wild-type Rad51 becomes significant after the addition of poly(dT) as DNA substrate, displaying saturation at a stoichiometry above 12 nt per monomer Rad51 protein (Figure 2C), again in agreement with previous analyses (4). The ATPase activity of Rad51-K342E protein was stimulated by the addition of poly(dT) by about 30%, saturating with a similar stoichiometry as wild-type protein (Figure 2C).

The Rad51–DNA complexes are dynamic under conditions of ATP hydrolysis, cycling between a high affinity DNA binding form when bound to ATP and a low-affinity binding form after ATP hydrolysis and nucleotide release (4). This feature of Rad51 protein necessitates stabilization of Rad51-DNA complexes for analysis by electrophoresis (Figure 5A, lanes 6 and 7). This dynamic behavior of Rad51 protein allows separating the DNA dependent and DNA–independent ATPase activities of the Rad51-K342E protein. Subtracting the DNA-independent ATPase activity from the total ATPase activity in the presence of poly(dT) (Figure 2D), revealed an identical profile of the ATPase activities of wild-type and Rad51-K342E proteins over a range of nt:protein stoichiometries. We also tested various DNA substrates in their ability to stimulate the ATPase activities of the wild-type and mutant Rad51 proteins (Figure 2E). The comparison is aided by subtracting the DNA-independent ATPase activity of Rad51-K342E (Figure 2F), showing a similar profile between the wild-type and mutant protein. Both proteins could not form ATPase-competent filaments on poly(dC) substrates. Both proteins preferred ssDNA over dsDNA. A significant decrease in the DNA-dependent ATPase activity was observed with Rad51-K342E for the poly(dA) and ϕX174 ssDNA substrates, as well as for dsDNA.

Although the Rad51-K342E protein purified exactly as the wild-type protein, we wanted to exclude the possibility that the Rad51-K342E preparation was contaminated with DNA. First, we showed that pre-incubation of Rad51-K342E protein with P1 nuclease did not affect its DNA-independent ATPase activity, showing that no DNA accessible to P1 was present in the protein preparation (Supplementary Figure 1). Second, UV spectra of the wild-type and mutant proteins did not reveal a nucleic acid absorption peak at 258 nm (data not shown). Third, [γ-^{32}P]-ATP labeling of the protein preparations directly or labeling of the aqueous phase after phenol extraction also failed to detect any DNA ends that could be labeled by kinase (data not shown).

We conclude that the DNA-independent ATPase activity of Rad51-K342E is a specific property of the mutant protein and not due to DNA contamination. Moreover, we conclude that the DNA-dependent ATPase activity of Rad51-K342E protein on poly(dT) is within error identical to the wild-type Rad51 protein. The reduced DNA-dependent ATPase activities of Rad51-K342E on specific ssDNA and dsDNA substrates are suggestive of a DNA-binding defect. These findings are corroborated by results of DNA-binding experiments (see below).

The Rad51-K342E DNA-independent ATPase activity is highly sensitive to ADP

To further establish differences between the DNA-independent and DNA-dependent ATPase activities of Rad51-K342E, we determined the sensitivity of the ATPase activity to product inhibition by ADP. ADP significantly inhibited the DNA-independent ATPase activity of Rad51-K342E protein in a protein-independent (Figure 3A) and ADP concentration-dependent (Figure 3B) manner. In the presence of 1 mM ATP, an equimolar amount of ADP inhibited activity over 4-fold and a 5-fold excess of ADP abolished activity (Figure 3B). In the presence of poly(dT) substrate, the DNA-dependent ATPase activity of wild-type and Rad51-K342E protein remained largely unaffected (Figure 3C and E). For better comparison, the DNA-independent ATPase activity of Rad51-K342E was subtracted from the total ATPase activity (Figure 3D). The effect of ADP on Rad51-K342E at the 1:1 stoichiometry is explained by the DNA-binding defect of the mutant protein and the ATPase activity under these conditions reflects the DNA-independent activity.

Titration of ADP to ATPase reactions containing DNA and the optimal nt:Rad51 (wild type or mutant) stoichiometry of 24:1 provided additional evidence for the existence of two distinct ATPase activities in the Rad51-K342E protein, one that is readily inhibited by low ADP concentrations and one that shows an identical inhibition profile to the wild-type protein requiring high ADP concentrations for inhibition (Figure 3F).

We conclude from these results that Rad51-K342E protein has two distinct ATPase activities, one DNA-independent and one DNA-dependent that can be distinguished by their sensitivity to product inhibition by ADP.

Rad51-K342E forms filaments in the absence of DNA

Since filaments represent the active form of RecA-like proteins, we reasoned that the Rad51-K342E mutant protein might be able to assemble into ATPase-competent filaments in the absence of a DNA lattice. Direct observation by electron microscopy (EM) revealed that Rad51-K342E forms filaments in the absence of DNA (Figure 4D) under conditions where wild-type Rad51 protein does not form filaments (Figure 4C).

In the presence of dsDNA and ATP + AlF_4^- Rad51-K342E forms long filaments (Figure 4B), which are indistinguishable from wild-type Rad51 filaments (Figure 4A). In the absence of DNA, when incubated with ATP + AlF_4^-, wild-type Rad51 protein does not form filaments (Figure 4C), whereas Rad51-K342E is capable of forming of filaments, albeit of shorter length than with dsDNA (Figure 4D). With ADP + AlF_4^- only Rad51-K342E rings were observed (Figure 4E). 3D reconstructions show that on dsDNA, Rad51-K342E protein forms extended filaments with a helical pitch of 97 Å (Figure 4G), which are similar to filaments formed by the Rad51 wild-type protein (Figure 4F). One difference was that the Rad51-K342E-DNA filaments show a

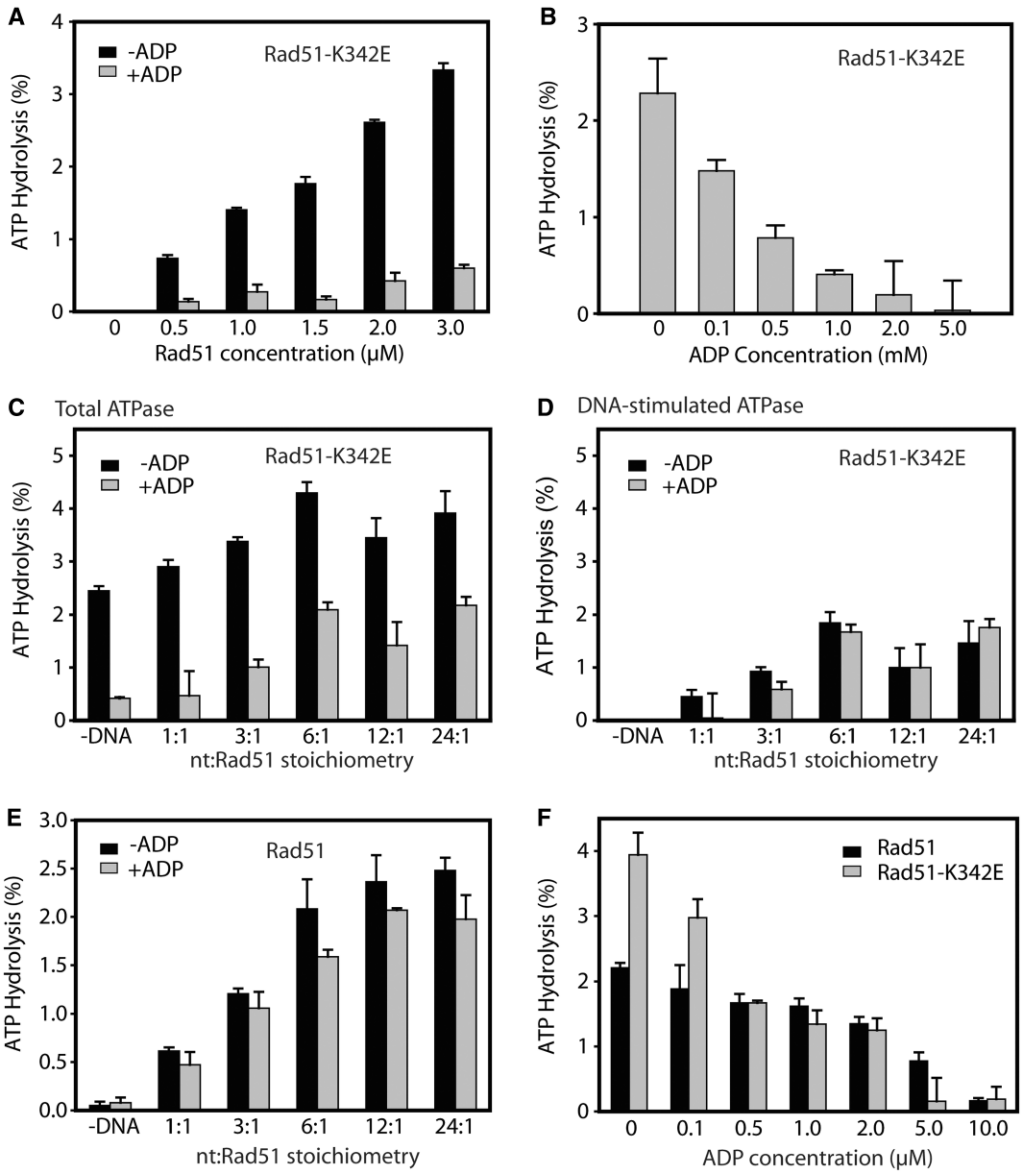

Figure 3. The DNA-independent ATPase activity of Rad51-K342E is sensitive to ADP. (**A**) DNA-independent ATPase activity at increasing concentration of Rad51-K342E protein in the presence or absence of 0.5 mM ADP. All reactions in (A–F) contain 1 mM ATP and 2 μM protein. (**B**) ADP titration of the DNA-independent ATPase activity of Rad51-K342E. (**C**) and (**E**) ADP inhibition of ATPase activity of Rad51-K342E and wild-type Rad51 protein, respectively, at fixed protein concentration (2 μM) and varying poly(dT) stoichiometry. (C) shows the total ATPase activity and (**D**) shows the DNA-stimulated Rad51-K342E ATPase activity, which was obtained after subtracting the ATPase activity in the absence of DNA from the values of the total ATPase activity. (**F**) Sensitivity of the ATPase activities of Rad51 and Rad51-K342E proteins (2 μM) to ADP in the presence of poly(dT) at a 1:24 Rad51:nt stoichiometry. Data shown are means ± 1 SD from three independent experiments.

smaller N-terminal lobe domain. In the absence of DNA, Rad51-K342E protein forms compressed filaments with a helical pitch of 81 Å (Figure 4H).

We conclude that Rad51-K342E protein forms filaments independent of a DNA lattice that show a shorter pitch than the extended filaments formed by the mutant and wild-type protein when bound to DNA.

Rad51-K342E displays a dsDNA-binding defect

Formation of a ternary complex with DNA and ATP is critical for the *in vivo* function of RecA-like proteins. Wild-type Rad51 forms complexes with both ssDNA and dsDNA in the presence of ATP that were visualized on agarose gels after glutaraldehyde fixation (Figure 5). Consistent with the defect in DNA-dependent ATPase activity using a dsDNA lattice [Figure 2F], Rad51-K342E displayed strongly diminished complex formation with dsDNA in the presence of ATP in this assay (Figure 5A). The effect is somewhat nucleotide cofactor dependent, as the defect was more pronounced with the slowly hydrolyzable ATP analog, ATP-γ-S (Figure 5B), but less pronounced with another non-hydrolyzable analog, ATP + AlF_4^- (Figure 5C). From control

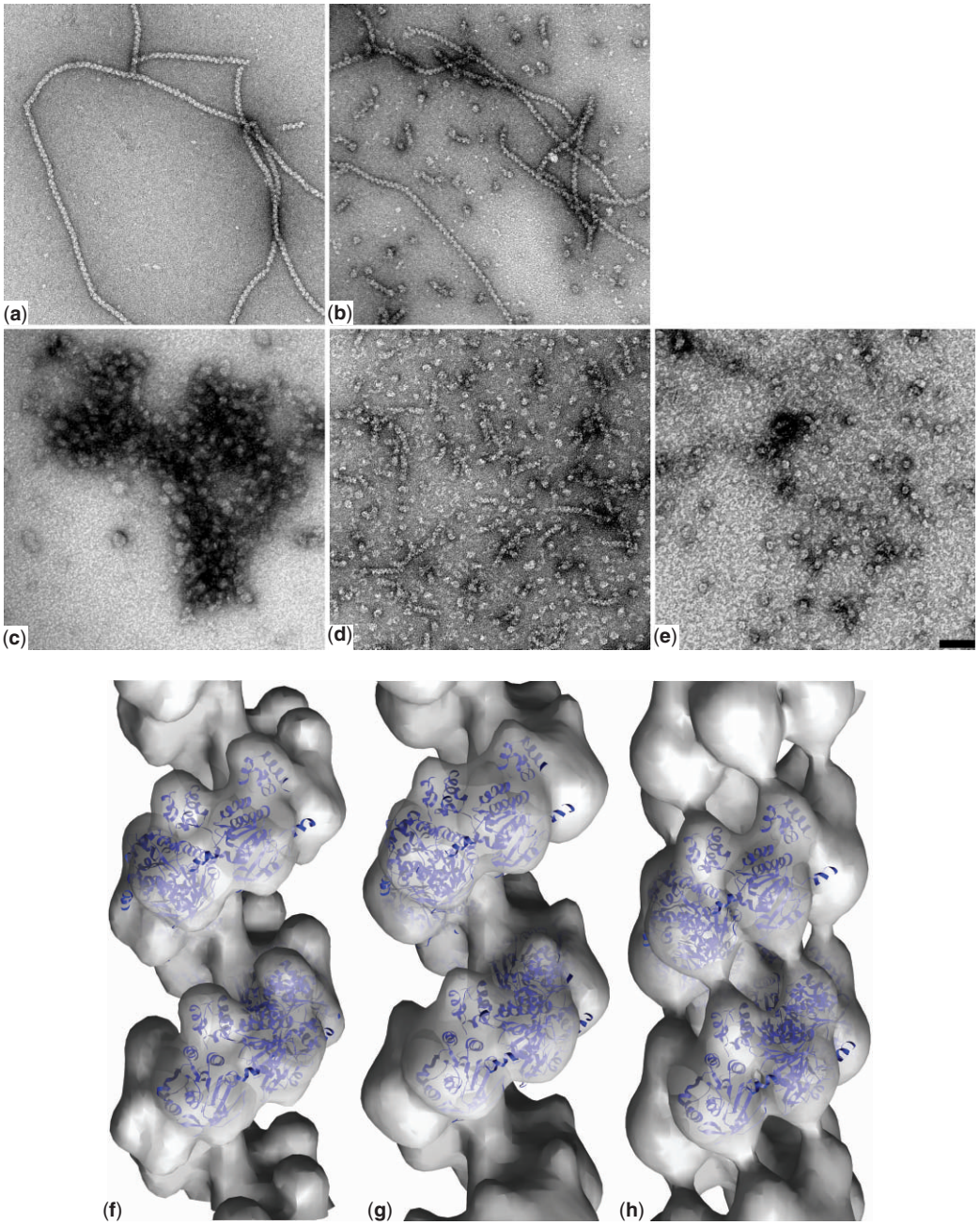

Figure 4. Rad51-K342E forms filaments in the absence of DNA. Filaments of wild-type Rad51 (**a**) and Rad51-K342E (**b**) in the presence of dsDNA and ATP + AlF_4^-. Filaments of Rad51-K342E are formed in the absence of DNA when incubated with ATP + AlF_4^- (**d**), whereas wild-type Rad51 protein does not form filaments under these conditions (**c**). Rings of Rad51-K342E form in the absence of DNA with ADP + AlF_4^- (**e**). All micrographs (A–E) are at the same magnification, scale bar = 50 nm. 3D reconstruction of wild-type Rad51 (**f**) and Rad51-K342E (**g**) filaments with dsDNA in the presence of ATP + AlF_4^-. In the absence of DNA, Rad51-K342E forms compressed filaments (**h**). The IHRSR method was used to generate 3D reconstructions from 8456 segments (each 332 Å long) of dsDNA-Rad51-K342E filaments (**g**), 3760 segments of Rad51-K342E filaments formed without DNA (h) and 3379 segments of wild-type Rad51 on dsDNA (f).

experiments we could infer that Rad51-K342E protein binds ATP-γ-S (data not shown).

The EM analysis showed that Rad51-K342E forms filaments on dsDNA in the presence of ATP + AlF_4^- (Figure 4B). These experiments were performed in the absence of the fixative glutaraldehyde, which is required to stabilize Rad51-dsDNA complexes formed in the presence of ATP that they can be analyzed on agarose gels. To emulate these conditions, we performed dsDNA-binding assays without fixative and found that Rad51-K342E formed complexes with dsDNA in the presence of ATP + AlF_4^- that withstood the electrophoresis conditions (Supplementary Figure 2).

With ssDNA, wild-type Rad51 protein formed large complexes that cannot be resolved on agarose gels, whereas Rad51-K342E protein formed complexes with

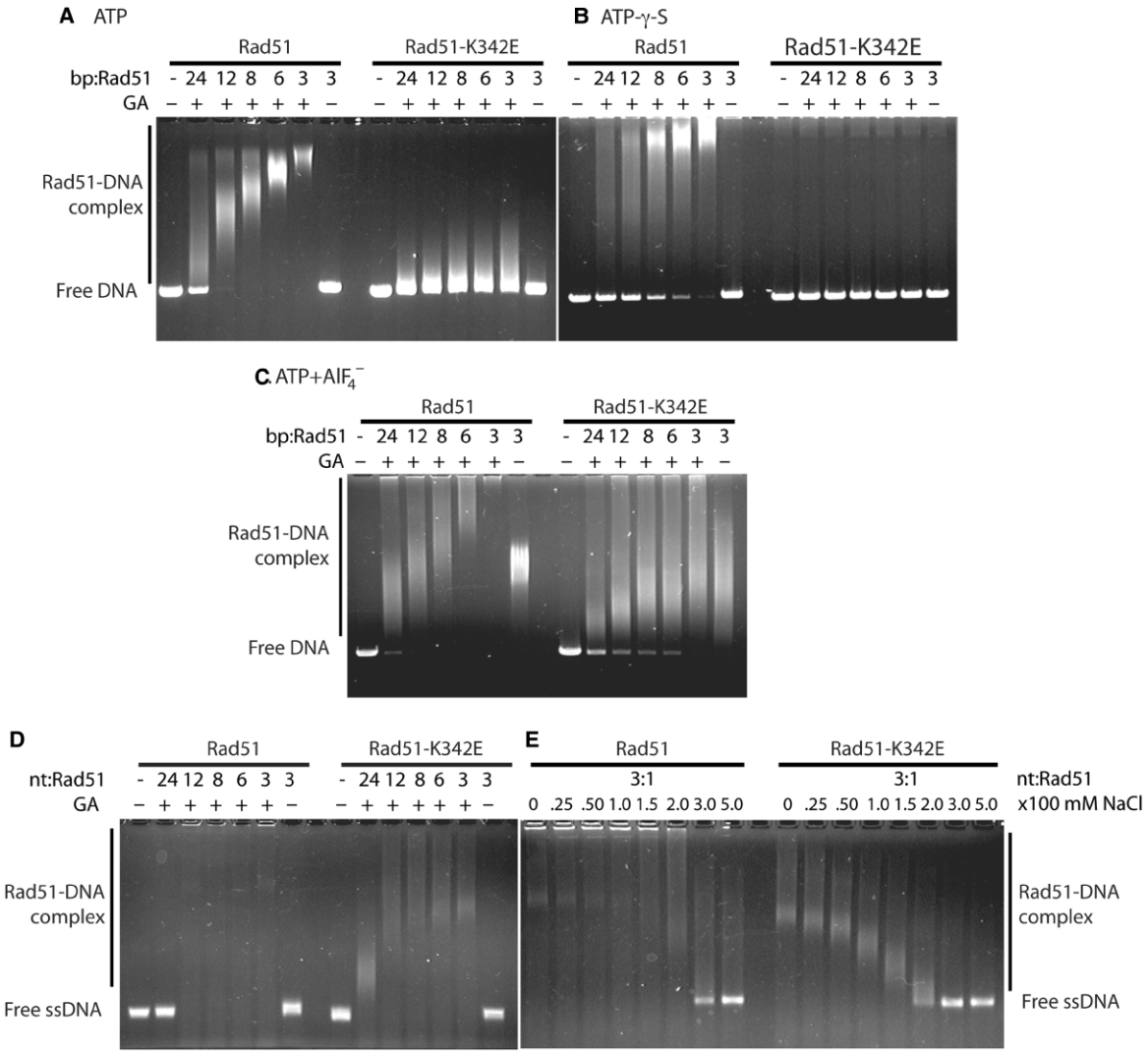

Figure 5. DNA-binding activity of Rad51-K342E. Rad51-K342E protein has a significant dsDNA-binding defect. Linear ϕX174 dsDNA (30 μM bp) was incubated with varying amounts of protein at the indicated stoichiometries in the presence of ATP (**A**), ATP-γ-S (**B**), or ATP + AlF_4^- (**C**) (5 mM each). Protein–DNA complexes were fixed by glutaraldehyde and separated on agarose gels. (**D**) Rad51-K342E protein has a slight ssDNA-binding defect. ϕX174 ssDNA (30 μM nt) was incubated with varying amounts of protein at the indicated stoichiometries in the presence of 5 mM ATP. (**E**) Salt titration of ssDNA binding by Rad51 and Rad51-K342E (10 μM) at a 3:1 stoichiometry. Rad51-ssDNA complexes were formed in the presence of increasing concentrations of NaCl (0–0.5M), crosslinked by glutaraldehyde and separated on agarose gels. GA, glutaraldehyde. GA does not affect the mobility of protein-free DNA under these conditions (data not shown).

faster mobility (Figure 5D). Interestingly, Rad51-K342E efficiently formed ssDNA complexes at a ratio of 24 nt per Rad51 monomer, that showed high mobility. Wild-type Rad51 failed to form stable complexes under these conditions (Figure 5D). Electrophoretic mobility of Rad51–DNA complexes reflects the degree of occupancy of Rad51 on the DNA lattice (27,39). This might suggest that the defect in Rad51–K342E DNA complex formation is not the initial binding but the formation of extended filaments. Consistent with this suggestion is the finding that salt titration revealed no significant difference in the salt sensitivity of ssDNA complex formation between the Rad51 and Rad51-K342E proteins (Figure 5E).

We conclude that Rad51-K342E displays a significant dsDNA-binding defect, whereas the defect in ssDNA binding is more subtle.

Rad51-K342E is competent for DNA strand exchange and is not inhibited by early addition of dsDNA

The key function of RecA-like proteins in homologous recombination is homology search and DNA strand exchange. This reaction can be recapitulated *in vitro* using the DNA strand exchange reaction (Figure 6A, top). Rad51-K342E is as competent as wild-type Rad51 to perform DNA strand exchange (Figure 6A), producing a similar amount of joint molecules and nicked circular products at the optimal protein to DNA ratio. This suggests that Rad51-K342E filament formation on ssDNA is sufficiently robust to perform homology search and DNA strand invasion. For reasons we do not understand our wild-type Rad51 protein consistently shows an optimum in the DNA strand exchange reaction at six nucleotides

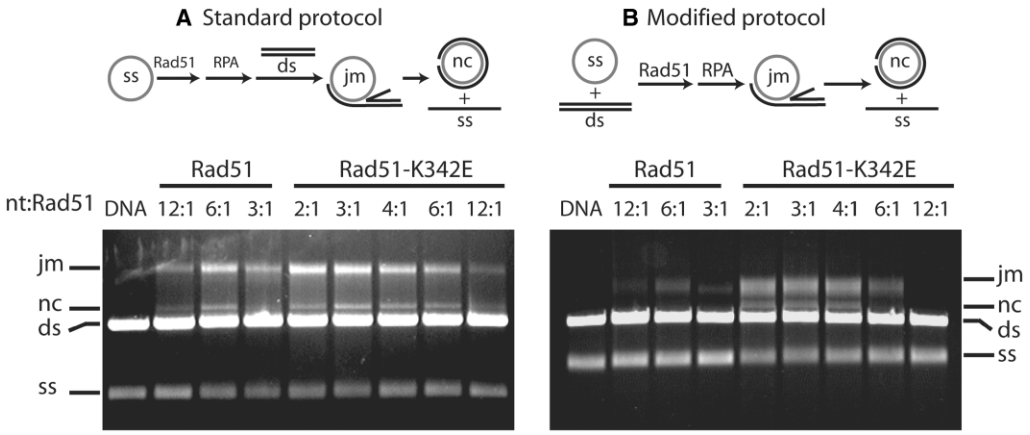

Figure 6. Rad51-K342E is competent for DNA-strand exchange activity. (**A**) *Top*: scheme of the standard protocol of the DNA strand-exchange reaction. Rad51 protein promotes the formation of joint molecules (jm) and nicked circular products (nc) from circular single-stranded DNA (ss) and homologous linearized double-stranded DNA (ds). The ssDNA (ϕX174 virion, 33 μM nt) was incubated with Rad51 at the indicate protein to ssDNA stoichiometry for 15 min to form Rad51-DNA filament, then RPA (1.8 μM) was added followed by 30 min incubation. Finally the linearized dsDNA (ϕX174 RFI, 33 μM bp) was added and the incubation was continued for 4 h. The mixture was deproteinized by adding a strand-exchange stopping buffer containing SDS and proteinase K and the mixtures were incubated at 30°C for 20 min. The different DNA species were visualized by ethidium bromide staining after electrophoresis on 0.8% agarose gels. (**B**) *Top*: scheme of the modified protocol of the DNA strand-exchange reaction, where Rad51 is co-incubated with ssDNA and dsDNA. Reactions were as in (A), except that the ssDNA and dsDNA were incubated with Rad51 at the same time for 15 min, then RPA was added and the incubation was continued for 5 h.

per protomer (Figure 6A)(23) rather than at the more typically found ratio of one protomer per three to four nucleotides. The Rad51-K342E protein shows a more typical optimum at three nucleotides per protomer ration, but the extent of the reaction is not significantly different from the wild-type protein at its optimum.

To examine the significance of the relatively stronger dsDNA-binding defect of the mutant protein, we used a modified protocol for the DNA strand exchange reaction. In the standard protocol, dsDNA is added after formation of the presynaptic filament, because early addition of dsDNA leads to Rad51 binding to dsDNA and inhibition of DNA strand exchange (Figure 6B). Co-incubation of Rad51 with ssDNA and dsDNA strongly inhibits DNA strand exchange by the wild-type protein (Figure 6B), consistent with previous observations (39). This biochemical feature of Rad51 DNA strand exchange activity poses a problem for the *in vivo* situation, where dsDNA is in large excess over ssDNA. Rad51-K342E protein, however, performed more efficient DNA strand exchange under these conditions (Figure 6B).

The DNA strand exchange activity of Rad51 protein is stimulated by Rad54 protein, involving species-specific protein interactions (39,40). There was no difference in the stimulation of DNA strand exchange between wild-type and K342E mutant Rad51 protein by Rad54 (data not shown).

In conclusion, Rad51-K342E protein performs DNA strand exchange *in vitro* as efficient as wild-type protein and is not subject to inhibition by the simultaneous presence of dsDNA during filament formation on ssDNA.

The Rad51-K342E - Rad54 interaction appears normal

The Rad51-K342E mutant was originally identified in a two-hybrid screen to enhance the interaction with Rad54 protein (20). The two-hybrid system measures protein–protein interaction in the context of a DNA-tethered fusion protein. The analysis of cognate budding yeast recombination proteins is complicated by the potential to interact with other nuclear proteins. To eliminate these confounding factors, we directly examined the interaction of Rad51-K342E with Rad54 in solution and on DNA. Analysis of the solution interaction between Rad51-K342E and Rad54 failed to identify an enhanced interaction between the wild-type and mutant Rad51 proteins (Supplementary Figure 3). Likewise, Rad51–K342E–dsDNA complexes showed a very similar profile and extent of stimulating the Rad54 ATPase activity (Supplementary Figure 4). The results do not provide evidence for an enhanced interaction between both proteins.

DISCUSSION

The biochemical properties of the *S. cerevisiae* Rad51-K342E mutant protein shed significant light on the function of L2 in Rad51. First, the significant dsDNA-binding defect evident in ATPase (Figure 2) and DNA-binding assays (Figure 5) as well as in the DNA strand exchange reaction (Figure 6) demonstrates a role of L2 in binding dsDNA to the primary DNA-binding site of Rad51. This may unveil a difference between the function of L2 between Rad51 and RecA. Second, the Rad51-K342E protein is proficient for DNA strand exchange (Figure 6), demonstrating that the secondary DNA binding is intact. Third, the ability of Rad51-K34E protein to form ATPase-competent filaments in the absence of a DNA lattice (Figures 2–4) suggests a key role of L2 to coordinate ATP binding with DNA binding and filament formation. Lastly, the enhanced interaction between Rad51-K342E and Rad54 in the two-hybrid

system is likely the indirect consequence of changes in the DNA-binding properties of the mutant Rad51 protein and it is unlikely that K342 is involved directly in Rad54 binding.

Rad51-K342E forms ATPase-competent filaments in the absence of DNA

Rad51-K342E protein displays distinct DNA-independent and DNA-dependent ATPase activities. The DNA-independent ATPase activity is defined by several criteria. First, the activity is not due to contaminating DNA, as several control experiments excluded the presence of DNA. Second, the DNA-independent filament exhibits a distinct pitch of 81 Å from the DNA-dependent filament with 97 Å. Third, EM image reconstruction revealed additional structural differences between both filaments (see Figure 5g versus h). Fourth, the DNA-independent ATPase is significantly more sensitive to product inhibition by ADP than the DNA-dependent filament. Based on the structural differences between both filament forms, we surmise that the DNA-independent filament subunit interface, which represents the ATP-binding pocket, is not as tightly closed as in the DNA-dependent filament. This would allow for faster nucleotide exchange with the ADP in solution. A high-resolution structure of the DNA-independent filament would be required to gain more insights. The ability of the Rad51-K342E mutant protein to form ATPase-competent DNA-independent filaments appears similar to the high salt activation of the RecA ATPase (41). However, RecA forms extended filaments with a 95 Å pitch under these conditions (42), identical to the pitch on DNA, whereas Rad51-K342E forms filaments with a compressed pitch compared to its filaments on DNA.

Loop 2 of Rad51 is involved in the primary DNA-binding site and coordinates ATP binding with DNA binding and filament formation

The DNA-binding sites of RecA protein were defined by cross-linking experiments and mutant protein analysis. A region of RecA protein overlapping with L2 crosslinks to ssDNA bound in the primary DNA-binding site (43), whereas another study found L1 and L2 residues (44). Under conditions allowing DNA binding in both the primary and secondary sites, neither L1 or L2 residues were found to crosslink to DNA, but rather the region between both loops (45). Lastly, another study using photo-crosslinking at different protein to DNA ratios determined L1 to be involved in the primary DNA-biding site and L2 in the secondary binding site (46). Analysis of the DNA-binding properties of a 20 residue peptide overlapping the L2 region indicated its involvement in the primary DNA-binding site (47–49). Also RecA mutant studies point to the involvement of L1 and L2 in DNA binding. The L1 mutant RecA-N99 (E156L/G157V) displayed biochemical properties consistent with an involvement in both the primary and secondary DNA-binding sites (50). Other L1 mutants, RecA1602 (G157D) and RecA1203 (R169C), were implicated in the binding of nucleotide cofactor (51). The L2 mutant RecA430 (G204S) exhibited DNA-binding properties indicating a role in the primary site (52,53), whereas another L2 mutant, RecA E207Q showed defect in the secondary DNA-binding site (54). The mutant and crosslinking studies do not allow a consistent assignment of the primary or secondary DNA-binding sites to L1 or L2. The recent RecA-ssDNA/dsDNA crystal structures demonstrate the involvement of L1 and L2 in the primary binding of ssDNA or dsDNA and provides insights how the three-stranded pairing intermediate might look (14). However, there is no structure of RecA yet, where both the primary and secondary DNA-binding sites are occupied and a potential pairing intermediate is trapped.

Significantly less information is available for Rad51. In the absence of crosslinking studies, Rad51 mutant analyses suggest the involvement of L1 and L2 in DNA binding. The L1 mutants in human Rad51 protein, Rad51-Y232A or W, exhibited a defect of binding ssDNA and dsDNA in the primary DNA-binding site (55). This involvement of L1 of Rad51 protein in DNA binding has been confirmed in further studies using a single molecule approach with hRad51-Y232A and hRad51-R235E (22). Prasad *et al.* (22) also studied mutants from the L2 region, the L2 mutant hRad51-K284A and the nearby hRad51-R303A, which were found to have little effect on primary site binding of DNA. Several mutants in L2 were shown to enhance ssDNA binding in the primary binding site of hRad51, including V269G and F279L, as well as the substitution of the residue immediately following L2, I287S (56). The budding yeast Rad51-I345T mutation also causes improved DNA binding and affects the homologous residue to hRad51-I287 (57). The central aromatic residue in L2 of RecA, F203, is critical for DNA binding and substitution with an alanine abolishes DNA binding of a mutant peptide (48); however, the analogous mutation in the context of the hRad51 protein, F279A, did not affect binding to ssDNA or dsDNA (55). Another L2 mutation, A272P, in the meiosis-specific RecA homolog, Dmc1, abolished D-loop formation due to a ssDNA-binding defect in the primary DNA-binding site (58).

The Rad51-K342E dsDNA-binding defect revealed a role of L2 in the primary DNA-binding site. The secondary DNA-binding site of Rad51-K342E appears largely intact, as indicated by the proficiency of the mutant protein to catalyze DNA strand exchange. The relative specificity of the DNA-binding defect for dsDNA is remarkable considering that the L2 structures in the RecA filaments assume a very similar conformation when bound to ssDNA or dsDNA (14). This suggests that the L2 region of eukaryotic Rad51 possesses additional features that contribute to specific interactions with dsDNA. There is little sequence conservation between L2 in RecA and Rad51 proteins and L2 in Rad51 proteins is longer (three amino acids in yeast; Figure 1B). It is possible that this difference in L2 contributes to the more avid binding of Rad51 to dsDNA compared to RecA. It will be interesting to see whether Rad51 L2 adopts different conformations when bound to ssDNA or dsDNA.

Previous analysis of mutants in L2 and the L2 region of hRad51 identified little effect on DNA binding to the primary site in several mutants, including K284A, R303A and F279A, suggesting to the authors that L2 does not contribute to filament formation on dsDNA (22,55). Residue K284 in hRad51 is the same as K342 in *S. cerevisiae* Rad51. The difference between hRad51-K284A and Rad51-K342E could be related to the difference in amino-acid substitution or to differences between the human and yeast Rad51 proteins. hRad51 requires a narrower definition of reaction conditions for efficient DNA strand exchange to curtail dsDNA binding (59) and uncontrolled ATPase activity (60). However, these changes largely affect the secondary binding site and not the binding to the primary site. The strict nucleotide cofactor requirement for DNA binding by yeast Rad51 at neutral pH is more relaxed in hRad51 (19,61), a difference in the primary DNA-binding site between both proteins. While this may contribute to the difference, we suggest that the primary reason for the strong defect in the yeast Rad51-K342E mutant compared to the hRad51-K284A mutant is the net loss of two positive charges by the charge change from a positive to a negative charge.

Analysis of the electrostatic potential of the Rad51 filament identifies a positively charged band that runs along the inner axis of the filament (Supplementary Figure 5). This charged band is composed of residues in the L1 and L2 regions (22). This general position of L1 and L2 is consistent with the structural data from *Escherichia coli* RecA (14), *Mycobacterium tuberculosis* RecA and *Methanococcus voltae* RadA (62,63), considering also contributions of the RecA C-terminus and Rad51 N-terminus to DNA binding (17,23,64). It appears likely that this positively charged band represents the primary and secondary DNA-binding site of the filament. In addition the N-terminal lobes of the Rad51 protomers (C-terminal lobe in bacterial RecA) form another non-continuous, right-handed helical band of positively charged patches (Supplementary Figure 5). Although the lobe domain is quite distant from L2 and may represent an independent DNA-binding site, there is significant flexibility in the connection between the lobe and the ATPase core, affording the possibility of an interaction between the lobe and the DNA-binding sites defined by L1 and L2. The definition of structural details and precise assignment awaits a co-crystal structure of the Rad51 filament with DNA.

The most intriguing feature of the Rad51-K342E mutant protein is its ability to form ATPase competent filaments in the absence of a DNA lattice. Binding to ATP or its non-hydrolyzable analog ATP + AlF_4^- triggered filament formation in the absence of DNA, suggesting that L2 coordinates ATP binding with filament formation and DNA binding. The definition of the L1 and L2 regions in the crystal structures of *M. tuberculosis* RecA and *M. voltae* RadA, as well as in the RecA-DNA complexes identified communication from the nucleotide co-factor binding site to L1 and L2 (14,62,63). The highly conserved Q195 residue of *M. tuberculosis* RecA, which sits at the beginning of L2 (see Figure 1B; residue 326 in *S. cerevisiae* Rad51), directly hydrogen bonds with the γ-phosphate oxygens and is proposed to trigger a conformational change in L2 to render the loop more ordered throughout the filament (63). This is consistent with the *M. voltae* RadA structure (62) and the role of the analogous Q194 residue in *E. coli* RecA (Figure 1B), which engages in an intermolecular hydrogen-bond network linking L2, DNA and co-factor in the RecA subunit interface (14). A role of the RecA Q194 residue in mediating a conformational change resulting from the binding of ATP had been proposed before (65) and biochemical analysis showed a key role of this residue in the allosteric regulation of RecA (66,67). Thus, it appears possible that the charge change in the Rad51-K342E protein mimics to some degree the DNA bound state, rationalizing how this L2 mutation leads to DNA-independent filament formation. However, as noted above the caveat is that the L2 sequence is poorly conserved (Figure 1B). While the anchoring NQ residues are fully conserved, the locations of the critical positively charged residues [e.g. RecA R196 (66)] are very different.

Rad51–Rad54 interaction

Rad51 and Rad54 are core factors in HR and their mutual interaction is critical for their function (68,69). In the two-hybrid system K342E was found to specifically enhance the interaction with Rad54 (20). Considering the location of L2, projecting towards the DNA-binding groove of the Rad51 filament, it appears unlikely that K342 is directly involved in Rad54 binding. Our previous EM studies showed that Rad54 associates with the ends of Rad51-dsDNA filaments (70). It would appear sterically impossible to involve the L2 region. Rather it seems likely that the structural differences in the Rad51-K342E-dsDNA complex evident from the EM 3D reconstruction (Figure 4), possibly represent a conformation that forms more stable complexes with Rad54 protein. It is unclear, why the Rad51-K342E mutant exhibits a hyper-rec effect in a recombination assay (21). It is possible that this effect is related to the reduced binding of the mutant protein to dsDNA. DNA strand exchange activity was enhanced compared to wild-type Rad51 in the simultaneous presence of ssDNA and dsDNA, a protocol that is likely a better mimic of the *in vivo* situation than the staged late addition of dsDNA in the standard protocol.

SUPPLEMENTARY DATA

Supplementary Data are available at NAR Online.

ACKNOWLEDGEMENTS

We thank Jachen Solinger and Stephen Kowalczykowski for providing purified RPA, Patrick Sung for plasmid pR51.3 and Xuan Li for Rad51-K191R protein. The helpful comments by Stephen Kowalczykowski and all members of the Heyer lab are gratefully acknowledged.

FUNDING

This work was supported by National Institutes of Health grant GM58015 (to W.D.H.), GM35269 (to E.H.E.) and

a Susan G. Komen Breast Cancer Foundation postdoctoral fellowship (PDF403213) to X.P.Z. Funding for open access charge: National Institutes of Health (Grant number R01 GM58015).

Conflict of interest statement. None declared.

REFERENCES

1. Heyer,W.D. (2007) In Aguilera,A. and Rothstein,R. (eds), *Molecular Genetics of Recombination*., Springer-Verlag, Berlin-Heidelberg, pp. 95–133.
2. Krogh,B.O. and Symington,L.S. (2004) Recombination proteins in yeast. *Annu. Rev. Genet*., **38**, 233–271.
3. Paques,F. and Haber,J.E. (1999) Multiple pathways of recombination induced by double-strand breaks in *Saccharomyces cerevisiae*. *Microbiol. Mol. Biol. Rev*., **63**, 349–404.
4. Bianco,P.R., Tracy,R.B. and Kowalczykowski,S.C. (1998) DNA strand exchange proteins: a biochemical and physical comparison. *Front. Biosci*., **3**, 570–603.
5. Kowalczykowski,S.C. (1991) Biochemistry of genetic recombination: energetics and mechanism of DNA strand exchange. *Annu. Rev. Biophys. Biophys. Chem*., **20**, 539–575.
6. Gupta,R.C., Folta-Stogniew,E., O'Malley,S., Takahashi,M. and Radding,C.M. (1999) Rapid exchange of A : T base pairs is essential for recognition of DNA homology by human Rad51 recombination protein. *Mol. Cell*, **4**, 705–714.
7. Folta-Stogniew,E., O'Malley,S., Gupta,R., Anderson,K.S. and Radding,C.M. (2004) Exchange of DNA base pairs that coincides with recognition of homology promoted by *E. coli* RecA protein. *Mol. Cell*, **15**, 965–975.
8. Howard-Flanders,P., West,S.C. and Stasiak,A. (1984) Role of RecA protein spiral filaments in genetic recombination. *Nature*, **309**, 215–219.
9. Mazin,A.V. and Kowalczykowski,S.C. (1996) The specificity of the secondary DNA binding site of RecA protein defines its role in DNA strand exchange. *Proc. Natl Acad. Sci. USA*, **93**, 10673–10678.
10. Mazin,A.V. and Kowalczykowski,S.C. (1998) The function of the secondary DNA-binding site of RecA protein during DNA strand exchange. *EMBO J*., **17**, 1161–1168.
11. Story,R.M., Weber,I.T. and Steitz,T.A. (1992) The structure of the *E. coli* recA protein monomer and polymer. *Nature*, **355**, 318–325.
12. Egelman,E.H. and Stasiak,A. (1986) Structure of helical RecA-DNA complexes. Complexes formed in the presence of ATP-gamma-S or ATP. *J. Mol. Biol*., **191**, 677–697.
13. Yu,X. and Egelman,E.H. (1993) The LexA repressor binds within the deep helical groove of the activated RecA filament. *J. Mol. Biol*., **231**, 29–40.
14. Chen,Z., Yang,H. and Pavletich,N.P. (2008) Mechanism of homologous recombination from the RecA-ssDNA/dsDNA structures. *Nature*, **453**, 489–484.
15. Conway,A.B., Lynch,T.W., Zhang,Y., Fortin,G.S., Fung,C.W., Symington,L.S. and Rice,P.A. (2004) Crystal structure of a Rad51 filament. *Nature Struct. Mol. Biol*., **11**, 791–796.
16. Ogawa,T., Yu,X., Shinohara,A. and Egelman,E.H. (1993) Similarity of the yeast RAD51 filament to the bacterial RecA filament. *Science*, **259**, 1896–1899.
17. Aihara,H., Ito,Y., Kurumizaka,H., Yokoyama,S. and Shibata,T. (1999) The N-terminal domain of the human Rad51 protein binds DNA: Structure and a DNA binding surface as revealed by NMR. *J. Mol. Biol*., **290**, 495–504.
18. Yu,X., Jacobs,S.A., West,S.C., Ogawa,T. and Egelman,E.H. (2001) Domain structure and dynamics in the helical filaments formed by RecA and Rad51 on DNA. *Proc. Natl Acad. Sci. USA*, **98**, 8419–8425.
19. Zaitseva,E.M., Zaitsev,E.N. and Kowalczykowski,S.C. (1999) The DNA binding properties of *Saccharomyces cerevisiae* Rad51 protein. *J. Biol. Chem*., **274**, 2907–2915.
20. Krejci,L., Damborsky,J., Thomsen,B., Duno,M. and Bendixen,C. (2001) Molecular dissection of interactions between Rad51 and members of the recombination-repair group. *Mol. Cell Biol*., **21**, 966–976.
21. Liu,L., Maguire,K.K. and Kmiec,E.B. (2004) Genetic re-engineering of *Saccharomyces cerevisiae* RAD51 leads to a significant increase in the frequency of gene repair *in vivo*. *Nucleic Acids Res*., **32**, 2093–2101.
22. Prasad,T.K., Yeykal,C.C. and Greene,E.C. (2006) Visualizing the assembly of human Rad51 filaments on double-stranded DNA. *J. Mol. Biol*., **363**, 713–728.
23. Zhang,X.P., Lee,K.I., Solinger,J.A., Kiianitsa,K. and Heyer,W.D. (2005) Gly-103 in the N-terminal domain of *Saccharomyces cerevisiae* Rad51 protein is critical for DNA binding. *J. Biol. Chem*., **280**, 26303–26311.
24. Sung,P. (1994) Catalysis of ATP-dependent homologous DNA pairing and strand exchange by yeast RAD51 protein. *Science*, **265**, 1241–1243.
25. Solinger,J.A., Lutz,G., Sugiyama,T., Kowalczykowski,S.C. and Heyer,W.-D. (2001) Rad54 protein stimulates heteroduplex DNA formation in the synaptic phase of DNA strand exchange via specific interactions with the presynaptic Rad51 nucleoprotein filament. *J. Mol. Biol*., **307**, 1207–1221.
26. New,J.H., Sugiyama,T., Zaitseva,E. and Kowalczykowski,S.C. (1998) Rad52 protein stimulates DNA strand exchange by Rad51 and replication protein A. *Nature*, **391**, 407–410.
27. Kiianitsa,K., Solinger,J.A. and Heyer,W.D. (2002) Rad54 protein exerts diverse modes of ATPase activity on duplex DNA partially and fully covered with Rad51 protein. *J. Biol. Chem*., **277**, 46205–46215.
28. Egelman,E.H. (2000) A robust algorithm for the reconstruction of helical filaments using single-particle methods. *Ultramicroscopy*, **85**, 225–234.
29. Thompson,J.D., Gibson,T.J., Plewniak,F., Jeanmougin,F. and Higgins,D.G. (1997) The CLUSTAL_X windows interface: flexible strategies for multiple sequence alignment aided by quality analysis tools. *Nucleic Acids Res*., **25**, 4876–4882.
30. Hall,T.A. (1999) BioEdit: a user-friendly biological sequence alignment editor and analysis program for Windows 95/98/NT. *Nucl. Acids Symp. Ser*., **41**, 95–98.
31. Marti-Renom,M.A., Stuart,A.C., Fiser,A., Sanchez,R., Melo,F. and Sali,A. (2000) Comparative protein structure modeling of genes and genomes. *Annu. Rev. Biophys. Biomol. Struct*., **29**, 291–325.
32. Sali,A. and Blundell,T.L. (1993) Comparative protein modelling by satisfaction of spatial restraints. *J. Mol. Biol*., **234**, 779–815.
33. Laskowski,R.A., MacArthur,M.W., Moss,D.S. and Thornton,J.M. (1993) PROCHECK: a program to check the stereochemical quality of protein structures. *J. Appl. Cryst*., **26**, 283–291.
34. Vriend,G. (1990) WHAT IF: a molecular modeling and drug design program. *J. Mol. Graph*., **8**, 52–56.
35. Sippl,M.J. (1993) Recognition of errors in three-dimensional structures of proteins. *Proteins*, **17**, 355–362.
36. Bowie,J.U., Luthy,R. and Eisenberg,D. (1991) A method to identify protein sequences that fold into a known three-dimensional structure. *Science*, **253**, 164–170.
37. Luthy,R., Bowie,J.U. and Eisenberg,D. (1992) Assessment of protein models with three-dimensional profiles. *Nature*, **356**, 83–85.
38. Roca,A.I. and Cox,M.M. (1997) RecA protein: structure, function and role in recombinational DNA repair. *Prog. Nucleic Acid Res. Mol. Biol*., **56**, 129–223.
39. Solinger,J.A., Kiianitsa,K. and Heyer,W.-D. (2002) Rad54, a Swi2/Snf2-like recombinational repair protein, disassembles Rad51:dsDNA filaments. *Mol. Cell*, **10**, 1175–1188.
40. Petukhova,G., Stratton,S. and Sung,P. (1998) Catalysis of homologous DNA pairing by yeast Rad51 and Rad54 proteins. *Nature*, **393**, 91–94.
41. Pugh,B.F. and Cox,M.M. (1988) High salt activation of recA protein ATPase in the absence of DNA. *J. Biol. Chem*., **263**, 76–83.
42. DiCapua,E., Ruigrok,R.W. and Timmins,P.A. (1990) Activation of recA protein: the salt-induced structural transition. *J. Struct. Biol*., **104**, 91–96.
43. Morimatsu,K. and Horii,T. (1995) DNA-binding surface of RecA protein photochemical cross-linking of the first DNA binding site on RecA filament. *Eur. J. Biochem*., **234**, 695–705.

44. Malkov,V.A. and Camerini-Otero,R.D. (1995) Photocross-links between single-stranded DNA and *Escherichia coli* RecA protein map to loops L1 (amino acid residues 157–164) and L2 (amino acid residues 195–209). *J. Biol. Chem.*, **270**, 30230–30233.
45. Rehrauer,W.M. and Kowalczykowski,S.C. (1996) The DNA binding site(s) of the *Escherichia coli* RecA protein. *J. Biol. Chem.*, **271**, 11996–12002.
46. Wang,Y. and Adzuma,K. (1996) Differential proximity probing of two DNA binding sites in the *Escherichia coli recA* protein using photo-cross-linking methods. *Biochemistry*, **35**, 3563–3571.
47. Gardner,R.V., Voloshin,O.N. and Camerini-Otero,R.D. (1995) The identification of the single-stranded DNA-binding domain of the *Escherichia coli* RecA protein. *Eur. J. Biochem.*, **233**, 419–425.
48. Voloshin,O.N., Wang,L.J. and Camerini-Otero,R.D. (1996) Homologous DNA pairing promoted by a 20-amino acid peptide derived from RecA. *Science*, **272**, 868–872.
49. Maraboeuf,F., Voloshin,O., Camerini-Otero,R.D. and Takahashi,M. (1995) The central aromatic residue in loop L2 of RecA interacts with DNA. Quenching of the fluorescence of a tryptophan reporter inserted in L2 upon binding to DNA. *J. Biol. Chem.*, **270**, 30927–30932.
50. Mirshad,J.K. and Kowalczykowski,S.C. (2003) Biochemical characterization of a mutant RecA protein altered in DNA-binding loop 1. *Biochemistry*, **42**, 5945–5954.
51. Wang,W.B. and Tessman,E.S. (1986) Location of functional regions of the *Escherichia coli* RecA protein by DNA sequence analysis of RecA protease-constitutive mutants. *J. Bacteriol.*, **168**, 901–910.
52. Menetski,J.P. and Kowalczykowski,S.C. (1990) Biochemical properties of the *Escherichia coli* recA430 protein. Analysis of a mutation that affects the interaction of the ATP-recA protein complex with single-stranded DNA. *J. Mol. Biol.*, **211**, 845–855.
53. Kawashima,H., Horii,T., Ogawa,T. and Ogawa,H. (1984) Functional domains of *Escherichia coli* recA protein deduced from the mutational sites in the gene. *Mol. Gen. Genet.*, **193**, 288–292.
54. Cazaux,C., Blanchet,J.S., Dupuis,D., Villani,G., Defais,M. and Johnson,N.P. (1998) Investigation of the secondary DNA-binding site of the bacterial recombinase RecA. *J. Biol. Chem.*, **273**, 28799–28804.
55. Matsuo,Y., Sakane,I., Takizawa,Y., Takahashi,M. and Kurumizaka,H. (2006) Roles of the human Rad51 L1 and L2 loops in DNA binding. *FEBS J.*, **273**, 3148–3159.
56. Kurumizaka,H., Aihara,H., Kagawa,W., Shibata,T. and Yokoyama,S. (1999) Human Rad51 amino acid residues required for Rad52 binding. *J. Mol. Biol.*, **291**, 537–548.
57. Fortin,G.S. and Symington,L.S. (2002) Mutations in yeast Rad51 that partially bypass the requirement for Rad55 and Rad57 in DNA repair by increasing the stability of Rad51–DNA complexes. *EMBO J.*, **21**, 3160–3170.
58. Bannister,L.A., Pezza,R.J., Donaldson,J.R., de Rooij,D.G., Schimenti,K.J., Camerini-Otero,R.D. and Schimenti,J.C. (2007) A dominant, recombination-defective allele of Dmc1 causing male-specific sterility. *PLoS Biol.*, **5**, 1016–1025.
59. Sigurdsson,S., Trujillo,K., Song,B.W., Stratton,S. and Sung,P. (2001) Basis for avid homologous DNA strand exchange by human Rad51 and RPA. *J. Biol. Chem.*, **276**, 8798–8806.
60. Bugreev,D.V. and Mazin,A.V. (2004) Ca^{2+} activates human homologous recombination protein Rad51 by modulating its ATPase activity. *Proc. Natl Acad. Sci. USA*, **101**, 9988–9993.
61. Chi,P., Van Komen,S., Sehorn,M.G., Sigurdsson,S. and Sung,P. (2006) Roles of ATP binding and ATP hydrolysis in human Rad51 recombinase function. *DNA Repair*, **5**, 381–391.
62. Wu,Y., Qian,X., He,Y., Moya,I.A. and Luo,Y. (2005) Crystal structure of an ATPase-active form of Rad51 homolog from *Methanococcus voltae*. Insights into potassium dependence. *J. Biol. Chem.*, **280**, 722–728.
63. Datta,S., Ganesh,N., Chandra,N.R., Muniyappa,K. and Vijayan,M. (2003) Structural studies on MtRecA-nucleotide complexes: insights into DNA and nucleotide binding and the structural signature of NTP recognition. *Proteins*, **50**, 474–485.
64. Aihara,H., Ito,Y., Kurumizaka,H., Terada,T., Yokoyama,S. and Shibata,T. (1997) An interaction between a specified surface of the C-terminal domain of RecA protein and double-stranded DNA for homologous pairing. *J. Mol. Biol.*, **274**, 213–221.
65. Story,R.M. and Steitz,T.A. (1992) Structure of the recA protein-ADP complex. *Nature*, **355**, 374–376.
66. Voloshin,O.N., Wang,L.J. and Camerini-Otero,R.D. (2000) The homologous pairing domain of RecA also mediates the allosteric regulation of DNA binding and ATP hydrolysis: A remarkable concentration of functional residues. *J. Mol. Biol.*, **303**, 709–720.
67. Kelley,J.A. and Knight,K.L. (1997) Allosteric regulation of RecA protein function is mediated by Gln194. *J. Biol. Chem.*, **272**, 25778–25782.
68. Heyer,W.D., Li,X., Rolfsmeier,M. and Zhang,X.P. (2006) Rad54: the Swiss Army knife of homologous recombination? *Nucleic Acids Res.*, **34**, 4115–4125.
69. Tan,T.L.R., Kanaar,R. and Wyman,C. (2003) Rad54, a Jack of all trades in homologous recombination. *DNA Repair*, **2**, 787–794.
70. Kiianitsa,K., Solinger,J.A. and Heyer,W.D. (2006) Terminal association of Rad54 protein with the Rad51-dsDNA filament. *Proc. Natl Acad. Sci. USA*, **103**, 9767–9772.